05,08

Microstructure of the thin iron films with perpendicular magnetic anisotropy

© N.M. Lyadov[1], I.R. Vakhitov[1,2], A.I. Gumarov[1,2], I.A. Faizrakhmanov[1], R.I. Khaibullin[1,2]

[1] Zavoisky Physical-Technical Institute, FRC Kazan Scientific Center of RAS,
Kazan, Russia
[2] Kazan Federal University,
Kazan, Russia

E-mail: nik061287@mail.ru

Received May 20, 2024
Revised June 4, 2024
Accepted June 4, 2024

Using high-resolution transmission electron microscopy and magnetometry we studied microstructure of the thin iron films with perpendicular magnetic anisotropy (PMA) and without it, formed by ion beam assisted deposition technique. It was established that iron films with PMA unlike films without PMA are nanocomposite film comprising iron nanoparticles with size 4−5 nm and paramagnetic iron oxide (FeO and Fe_2O_3). In general the data obtained indicate that the key role in PMA belongs to nanocomposite structure of films with weak exchange-coupled ferromagnetic nanoparticles of iron in paramagnetic matrix.

Keywords: ion beam assisted deposition, nanocomposite, electron microscopy, magnetic properties.

DOI: 10.61011/PSS.2024.08.59054.127

1. Introduction

The thin ferromagnetic films with perpendicular magnetic anisotropy (PMA) are of increased interest due to their probable use in magnetic-sensing devices of spintronics and straintronics [1–4]. It is well known that structure, magnetic and phase composition, and thickness of thin ferromagnetic films are basic factors determining their magnetic characteristics, and in particular magnetic-anisotropic properties, including PMA. For example, the epitaxial films of ferromagnetic materials with thickness of several atomic layers, formed by method of molecular-beam epitaxy, demonstrate the spin-oriented transition having quantum nature [5,6]. Another example is ferromagnetic thin films with column structure [7,8]. Such films are also characterized by PMA presence, and its mechanism is linked with magnetic anisotropy of shape. Magnetostriction, as mechanism of PMA occurrence, also plays significant role. As example we can provide the results of own studies of nickel films, deposited by ion beam assisted deposition technique [9]. The nickel films 200−300 nm thick of substrate of melted quartz after thermal annealing in vacuum demonstrated PMA, this was associated occurrence on the nickel film of the tension macrostresses. There are examples when PMA of thin films is due to magnetocrystalline anisotropy [10]. So, mechanism of PMA occurrence in thin films can be of different physical nature, and what of them „works“ in each given case is not always apparent, but his exactly determines the scope of practical application of the ferromagnetic films with PMA.

Obviously the structure and phase composition of thin films, including ferromagnetic, depend, by actually — are determined by the method and conditions of their deposition. The deposition conditions mean a large set of parameters: residual vacuum, deposition rate, substrate temperature, its structural parameters, purity of precursors, etc. Among the ion-plasma methods of deposition of thin ferromagnetic films the ion beam assisted deposition (IBAD) is the most promising in terms of the process control [11].

Previously in our papers [12,13] we provide the study results of structure and magnetic properties of thin films of iron 100−300 nm thick obtained by IBAD method. Based on X-ray structural studies it was established that the iron films are nanocrystalline and textured. Average size of crystallites α-Fe is ~ 5 nm with predominant orientation of planes (110) of iron crystallites parallel to the plane of the substrate. It was determined that the iron nanocrystallites have significant homogeneous deformation ($\sim 2.6\%$). The iron films demonstrated PMA depending on the deposition rate, this is confirmed by the magnetic hysteresis loop with transcritical shape, and stripe domain structure [14–17]. Studies of the elemental composition by method of X-ray photoelectron spectroscopy and of the phase composition using such methods as X-ray and electron diffraction, Mössbauer spectroscopy of conversion electrons and thermomagnetic analysis showed presence in films with PMA of significant amount of oxygen and paramagnetic (at room temperature) iron oxide FeO. Iron films without PMA, obtained at relatively high deposition rates, did not contain additional iron oxide phases in their composition.

Currently the available set of experimental data do not allow to make firm conclusion on the mechanism of PMA occurrence in thin films of iron deposited by IBAD technique. Due to this the present paper task is

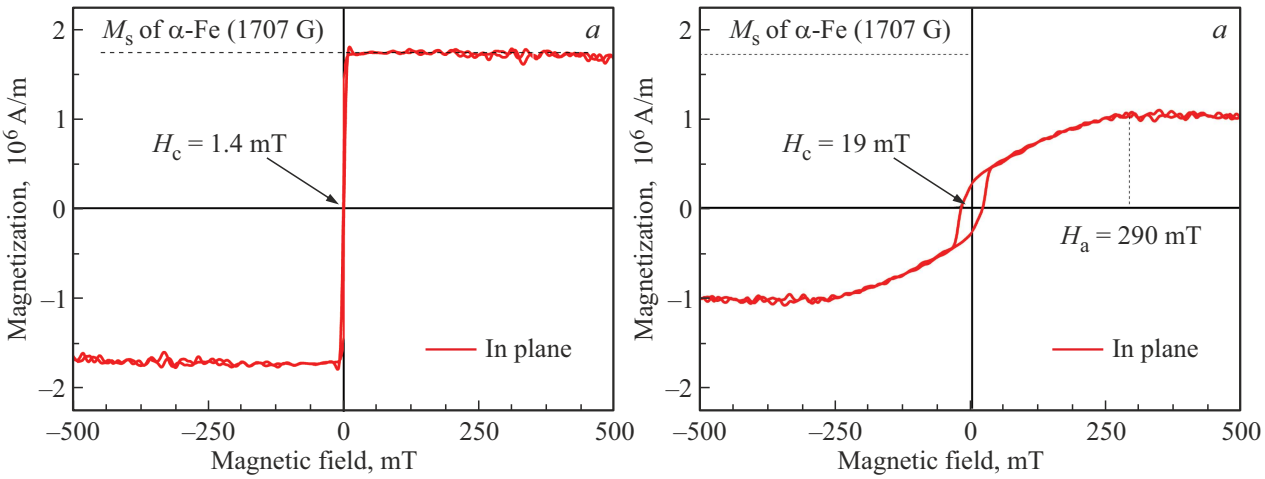

Figure 1. Dependencies of magnetization of iron films *a*) without PMA (Fe-1) and *b*) with PMA (Fe-2). M_s — saturation magnetization, H_c — coercive field, H_a — anisotropy field.

(comparative) study of microstructure of the thin iron films with and without PMA by high resolution transmission electron microscopy (HR TEM) technique (HR TEM).

2. Experimental procedure

The iron thin films were deposited by IBAD technique on substrates of single crystal silicon (111). Preliminary the substrates were degreased (wiped with ethyl alcohol), washed with distilled water and annealed in air at temperature $\sim 400^\circ$C for 1 h. For deposition of the iron thin films the iron target with diameter 65 mm was used, it was sputtered by flow of xenon ions Xe^+. Ions flow was created by a Kaufman-type ion source. Xenon with purity 99.995% was used as the working gas. Xenon ions energy was 1 keV. Films were deposited in vacuum $2 \cdot 10^{-2}$ Pa. Base pressure in vacuum chamber i. e. pressure before working gas supply in the ion source was $1-2 \cdot 10^{-3}$ Pa. The substrate temperature during films deposition do not exceed 50°C. Details of the experimental deposition method were described in detail in paper [13]. Iron films studied in this paper were deposited at rates 9 (sample Fe-1) and 3.2 nm/min (sample Fe-2). The deposition rate was controlled by density of the ion current. Density of ion current for samples Fe-1 and Fe-2 was 150 and 65 μA/cm^2 respectively. As result samples of thin films of iron $\sim 100-120$ nm thick were obtained.

The surface morphology and elemental composition of the films were studied, and the film thickness was measured in scanning electron microscope (SEM) EVO 50 XVP with the X-ray energy-dispersive spectrometer Inca Energy-350 equipped in SEM vacuum chamber. The structure and phase composition were studied by X-ray diffraction in Bragg and grazing geometry using a Dron-7 diffractometer with a Cukα source and β-filter. Dependence of films magnetization on magnetic field (magnetic hysteresis loop) at room temperature was measured in magnetometer with magnetic field sweep to 500 mT [18], and in unit PPMS-9 by method of vibrational magnetometry in temperature range 4–300 K. Dimensions of samples for magnetic measurements were $\sim 5.0 \times 5.0$ mm^2.

Microstructure of films (cross section) were studied by HR TEM on Titan electron microscope (Thermo Fisher Scientific).

3. Results and discussion

Elemental composition, magnetic properties and structure were studied of the samples of iron thin films Fe-1 and Fe-2. The elemental analysis showed that oxygen content in sample Fe-1 is ~ 4 at.%, and in sample Fe-2 ~ 21 at.%. Data of X-ray diffraction analysis show that samples are textured, predominantly with orientation of planes (110) of iron crystallites in parallel with substrate plane. Average size of iron crystallites is ~ 5.5 nm. Besides, films contain unordered component α-Fe ($\sim 24\%$). Sample Fe-2, additionally to metal iron α-Fe contains phase FeO. Iron oxide is formed in iron film during deposition due to residual oxygen of vacuum chamber at relatively low deposition rates. If we base on the sample elemental composition then content in percent of phase FeO is $\sim 40\%$. This value is close to the threshold of percolation for the composite materials of type metal–dielectric.

Figure 1 shows the magnetic hysteresis loops which indicate that sample Fe-2 has PMA (field PMA $H_a = 290$ mT), and saturation magnetization is significantly lower as compared to α-Fe and is $\sim 60\%$ of saturation magnetization of α-Fe. as expected, the sample Fe-2 with PMA is nonuniform by both structure, and phase composition, and significantly differs from sample Fe-1 without PMA.

Figure 2, *a* and *b* shows overview dark-field TEM images of the cross sections of thin films of iron without PMA (sample Fe-1) and with PMA (sample Fe-2). Dark-field TEM-images were obtained by selection of a small sector

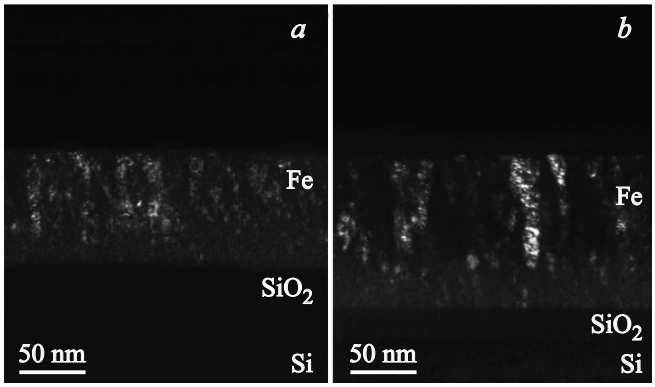

Figure 2. Dark-field image of transverse sections of iron films: *a*) without PMA and *b*) with PMA.

by diaphragm on an intense ring of electron microdiffraction from planes (110) α-Fe (interplanar spacing $d \approx 2.05$ Å). Due to this in dark-field TEM-images we observed contrasting of finely dispersed particles of phase α-Fe with planes (110) perpendicular to the substrate. The overview photo (Figure 2, *b*) of sample Fe-2 shows oxide layer of silicon ~ 20 nm thick. This layer formed on the surface of the silicon substrate during its annealing in air. The dark-field image of sample Fe-1 (Figure 2, *a*) is generally less contrast — probably due to larger thickness of the transverse section, as result the oxide layer of silicon is not visible on it. This version if confirmed by the fact that sample Fe-2 also with movement to center of the etching pit to the periphery the contrast in photo between the silicon oxide layer and silicon disappears. Further photos of the cross sections of both samples have no differences: layer 20−25 nm thick is observed, it comprises fine dispersed particles of iron which is directly adjacent to the substrate, and above this layer the layer of more coarse mutually oriented iron nanocrystals is observed.

Figure 3 shows light-field high resolution TEM-images of cross sections and patterns of electron microdiffraction for samples Fe-1 without PMA (*a, b*) and Fe-2 with PMA (*c, d*). The diffraction ring (110) (Figure 3, *b* and *d*) α-Fe comprises areas of increased intensity and blurred areas that can be attributed to iron nanocrystallites and intercrystalline disordered regions of iron. The interplanar spacing is 2.03−2.05 Å, this corresponds to d_{110} for α-Fe. This agrees well with the results of previous studied made by TEM method [12] and by X-ray diffraction analysis of iron films [13]. The pattern of electronic microfiffraction of sample Fe-2 contains additional reflexes, which can be attributed to phases of iron oxide FeO and Fe_3O_4. At the same time, a relatively large spread of interplanar spacings for the oxide phase is observed in different areas of iron films with PMA (sample Fe-2), which can be attributed to magnetite (Fe_3O_4) or hematite (Fe_2O_3). The pattern of electronic microdiffraction for sample Fe-2 (Figure 3, *d*) contains also intensive reflex from planes (111) FeO with $d_{111} \approx 2.5-2.6$ Å. Other intensive reflexes from oxide phase FeO, such as (200) and (220), which relative density is 100 and 53% [19], are not observed. Probably this is associated with the textured rise of the oxide phase also. The reflex with $d \approx 2.5-2.6$ Å can be attributed to hematite Fe_2O_3 ($d_{110} = 2.519$ Å) [19]. But, considering the previously obtained results of the X-ray diffraction analysis of iron thin films samples with PMA [13], we can state that FeO is oxide phase.

Figure 3, *a* presents fragment of TEM-image of microstructure of sample Fe-1 obtained under high-resolution mode. Photo shows crystal planes (110) α-Fe, spacing between them is 2.06−2.08 Å. The planes have different orientation relative to horizontal line of the photo. Boundaries between nanocrystallites are shown poorly, and this makes it difficult their size and shape. Besides, the film comprises significant portion of disordered iron phase.

Figure 3, *c* presents fragment of TEM-image of microstructure of sample Fe-2 obtained under high-resolution mode. Photo shows crystallites with different orientation of crystal planes, and disordered regions. The interplanar spacings are about 2.1 Å despite on crystallite orientation, this is close by value to the interplanar spacing d_{110} for α-Fe. On the other hand, 2.1 Å is close to value of interplanar spacing $d_{200} = 2.15$ Å of FeO. Since the nanocrystals in the analyzed layer are located with a random orientation (rings in the diffraction pattern), the electrons pass through stacks of nanocrystals (moire is visible in the HR TEM-images). So, it was impossible to distinguish nanocrystals Fe and FeO by different scattering or absorption of electrons. As for shape the nanocrystals are elongated, and their size is $\sim 5 \times 10\,\text{nm}^2$. Besides, the fulls-scale photo also shows the crystal planes with $d \approx 1.43$ Å, this corresponds to planes (200) α-Fe.

So, electron microscopy even in high resolution mode ensures determination of the details of microstructure of iron films with PMA. It was expected that the presence of large portion of the oxide phase paramagnetic at room temperature in the sample Fe-2 with PMA shall lead to the formation of nanocomposite film with ferromagnetic nanoparticles α-Fe in nonmagnetic matrix. Due to this reason we measured the temperature dependencies of magnetization of samples Fe-1 and Fe-2 during their cooling in magnetic field (FC) and without field (ZFC), which are shown in Figure 4, *a* and *b*. This method is rather informative during studies of the composite magnetic materials, as it ensures provides data on magnetic microstructure of the material [15,20].

Practically monotonic temperature dependences of magnetization ZFC and FC ($H = 5$ Oe) of sample Fe-1 confirm the homogeneity of its magnetic structure. In region $T = 45$ K a small feature (Figure 4, *a*) is observed, which is determined, as we suppose, by nanoparticles of iron in region of the transition layer film−substrate (Figure 2, *a*). Dependences ZFC and FC ($H = 50$ Oe) of sample Fe-2 have more complex non-monotonic nature and were not observed previously (Figure 4, *b*). In temperature range 4−170 K dependences ZFC and FC are typical for nanocomposite

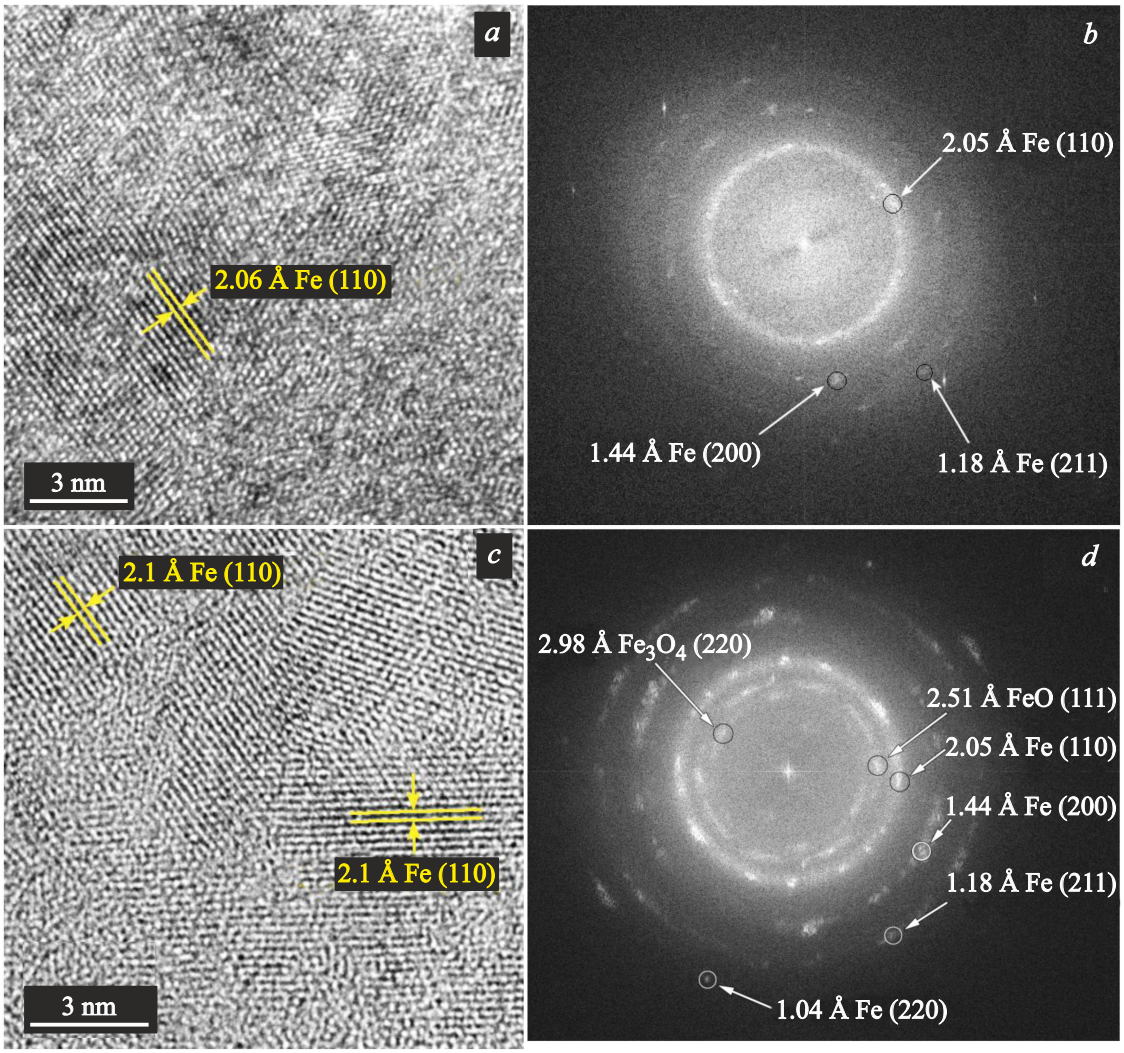

Figure 3. Light field images and microdiffraction of the transverse sections of samples of thin films of iron Fe-1 without PMA (*a, b*) and Fe-2 with PMA (*c, d*).

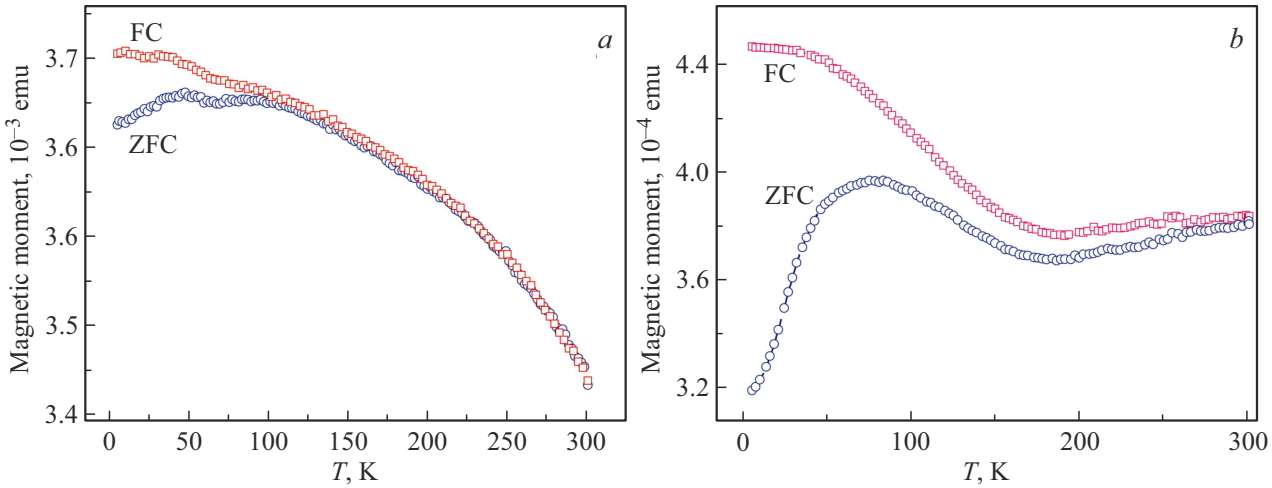

Figure 4. Magnetic moment vs. temperature during cooling in weak magnetic field (FC) and without field (ZFC) of samples of iron films *a*) Fe-1 without PMA and *b*) Fe-2 with PMA.

materials with weakly interacting ferromagnetic nanoparticles (see for example [20]). Interlock temperature T_b (position of maximum on dependence ZFC, Figure 4, *b*) is about 77 K. Using expression

$$25k_{\mathrm{B}}T_b = K_{\mathrm{a}}V_{\mathrm{av}},$$

where k_{B} — Boltzmann's constant, T_b — interlock temperature, K_{a} — magnetic anisotropy constant ($\sim 10^7$ erg/cm^3 for nanoparticles, which average diameter is below ~ 10 nm) [21–23], by average volume of nanoparticle V_{av} we can estimate the average size of nanoparticles of iron in sample with PMA, which was ~ 4 nm, this agrees with results of study by HR TEM method (see above). Estimation of nanoparticles size from width of X-ray reflex gives ~ 5.5 nm, this well agrees with provided estimation. In temperature range 170−300 K magnetization increasing in both temperature dependences (ZFC and FC) is observed. We expect, that this is due to presence in sample of „large" ferromagnetic nanoparticles of iron, strong magnetic interaction is between them. Taking as temperature of magnetic inconvertibility T_{irr} the point of crossing of dependences ZFC and FC ($T_{\mathrm{irr}} \approx 300$ K) [20], we can estimate the average size of these particles, which is ~ 6 nm.

4. Conclusion

Structure and phase composition of iron thin films formed by IBAD technique are inhomogeneous. There is strip of fine dispersed iron particles which is directly adjacent to the substrate. Above this strip there are coarsening of nanocrystals α-Fe and their oriented growth. The iron films with PMA unlike films without PMA are nanocomposite comprising iron nanoparticles with size 4−5 nm and iron oxide (FeO). The obtained data confirm the previous conclusion on the mechanism of PMA occurrence in iron thin films formed by IBAD technique [12,13]. Namely, this homogeneous microdeformation of iron nanocrystalllites, which results in occurrence of additional magnetic moment in all directions due to magnetic elastic effect. Averaging of these moments in the film plane gives zero due to random orientation of the iron crystallites. But due to films texture the induced magnetic moment of the nanocrystallites in perpendicular direction is summed. As result PMA occurs.

Acknowledgments

The authors thank V.I. Vdovin and A.K. Gutakovsky for TEM studies at the Rzhanov Institute of Semiconductor Physics of Siberian Branch of RAS.

Funding

The present work was performed under the state assignment of FRC Kazan Scientific Center of RAS. Part of the work of I.R. Vakhitov and A.I. Gumarov was carried out at the Kazan (Volga Region) Federal University.

Conflict of interest

The authors declare that they have no conflict of interest.

References

[1] S.A. Wolf, D.D. Awschalom, R.A. Buhrman, J.M. Daughton, S. von Molnar, M.L. Roukes, A.Y. Chtchelkanova, D.M. Treger. Sci. **294**, *5546*, 1448 (2001).
[2] I. Žutić, J. Fabian, S.D. Sarma. Rev. Mod. Phys. **76**, *2*, 323 (2004).
[3] A.A. Bukharaev, A.K. Zvezdin, A.P. Pyatakov, Y.K. Fetisov. Phys. — Usp. **61**, *12*, 1175 (2018).
[4] S. Bandyopadhyay. Magnetic Straintronics. Springer, Switzerland (2022). P. 135.
[5] D.P. Pappas, K.P. Kämper, H. Hopster. Phys. Rev. Lett. **64**, *26*, 3179 (1990).
[6] Z. Celinski, B. Heinrich. J. Appl. Phys. **70**, *10*, 5935 (1991).
[7] L. Xi, J.M. Lu, J.J. Zhou, Q.J. Sun, D.S. Xue, F.S. Li. J. Magn. Magn. Mater. **322**, *15*, 2272 (2010).
[8] A.I. Linnik, A.M. Prudnikov, R.V. Shalaev, V.N. Varyukhin, S.A. Kostyrya, V.V. Burkhovetskii. Tech. Phys. Lett. **38**, *6*, 499 (2012).
[9] N.M. Lyadov, V.V. Bazarov, I.R. Vakhitov, A.I. Gumarov, S.Z. Ibragimov, D.M. Kuzina, I.A. Faizrakhmanov, R.I. Khaibullin, V.A. Shustov. Phys. Solid State **63**, *11*, 1723 (2021).
[10] A.V. Petrov, S.I. Nikitin, L.R. Tagirov, A.S. Kamzin, R.V. Yusupov. JETP Lett. **118**, *2*, 117 (2023).
[11] J.K. Hirvonen. Mater. Sci. Rep. **6**, *6*, 215 (1991).
[12] N.M. Lyadov, V.V. Bazarov, F.G. Vagizov, I.R. Vakhitov, E.N. Dulov, R.N. Kashapov, A.I. Noskov, R.I. Khaibullin, V.A. Shustov, I.A. Faizrakhmanov. Appl. Surf. Sci. **378**, 114 (2016).
[13] N.M. Lyadov, F.G. Vagizov, I.R. Vakhitov, A.I. Gumarov, Sh.Z. Ibragimov, D.M. Kuzina, I.A. Faizrakhmanov, R.I. Khaibullin, V.A. Shustov. Vacuum **168**, 108860 (2019).
[14] V.I. Halauchuk, Y.A. Bumai, M.G. Lukashevich, N.M. Lyadov, I.A. Faizrakhmanov, R.I. Khaibullin. Phys. Solid State **64**, *14*, 2324 (2022).
[15] P. Sharma, H. Kimura, A. Inoue, E. Arenholz, J.-H. Guo. Phys. Rev. B **73**, *5*, 052401 (2006).
[16] P. Sharma, H. Kimura, A. Inoue. J. Appl. Phys. **101**, *9*, 09N502 (2007).
[17] M. Coísson, F. Celegato, E. Olivetti, P. Tiberto, F. Vinai, M. Baricco. J. Appl. Phys. **104**, *3*, 033902 (2008).
[18] D.K. Nurgaliev, P.G. Yasonov. Koertsitivny spektrometr. Patent RF na poleznuyu model' № 81805. Bul. FIPS № 9 (2009). (in Russian).
[19] L.I. Mirkin. Spravochnik po rentgenosrukturnomu analizu polikristallov. Fizmatgiz, M. (1961). S. 863. (in Russian).
[20] L. Machala, R. Zboril, A. Gedanten. J. Phys. Chem. B **111**, *16*, 4003 (2007).
[21] G.I. Frolov. Tech. Phys. **74**, *7*, 909 (2004).
[22] N.M. Dempsey, L. Ranno, D. Givord, J. Gonzalo, R. Serna, G.T. Fei, A.K. Petford-Long, R.C. Doole, D.E. Hole. J. Appl. Phys. **90**, *12*, 6268 (2001).
[23] Z.M. Zeng, P. Khalili Amiri, J.A. Katine, J. Langer, K.L. Wang, H.W. Jiang. Appl. Phys. Lett. **101**, *6*, 062412 (2012).

Translated by I.Mazurov